Constraining viewing geometries of pulsars with single-peaked γ-ray profiles using a multiwavelength approach

A S Seyffert[1]**, C Venter**[1]**, T J Johnson**[2,3] **and A K Harding**[2]

[1] Centre for Space Research, North-West University, Potchefstroom Campus, Private Bag X6001, Potchefstroom 2520, South Africa
[2] Astrophysics Science Division, NASA Goddard Space Flight Center, Greenbelt, MD 20771, USA
[3] Department of Physics, University of Maryland, College Park, MD 20742, USA

E-mail: 20126999@nwu.ac.za

Abstract. Since the launch of the Large Area Telescope (LAT) on board the *Fermi* spacecraft in June 2008, the number of observed γ-ray pulsars has increased dramatically. A large number of these are also observed at radio frequencies. Constraints on the viewing geometries of 6 γ-ray pulsars exhibiting single-peaked γ-ray profiles were derived using high-quality radio polarization data [14]. We obtain independent constraints on the viewing geometries by using a geometric emission code to model the *Fermi* LAT and radio light curves (LCs). We find fits for the magnetic inclination and observer angles by searching the solution space by eye. Our results are generally consistent with those previously obtained [14], although we do find differences in some cases. We will indicate how the γ-ray and radio pulse shapes as well as their relative phase lags lead to constraints in the solution space. Values for the flux correction factor (f_Ω) corresponding to the fits are also derived (with errors).

1. Introduction

We study 6 pulsars (J0631+1036, J0659+1414, J0742−2822, J1420−6048, J1509−5850, and J1718−3825) detected by *Fermi* LAT, all exhibiting single-peaked pulse profiles within current statistics at energies > 0.1 GeV. These pulsars are also detected in the radio band. Both of these properties aid in constraining the possible solution space for the respective pulsar geometries, as derived from predictions of their light curves (LCs).

A study of the pulsars' geometric parameters, the inclination and observer angles α and ζ, has been performed [14] using the radio polarization and LC data. They constrained the solution space for α and β of the individual pulsars, with $\beta = \zeta - \alpha$, using fits to these radio data as well as predictions for the value of the half opening angle of the radio beam derived from the radio pulse width (e.g., [6]).

The aim of this study is to obtain similar constraints on α and ζ of the same pulsars using an independent, multiwavelength approach. We use a geometric pulsar emission code (e.g., [12]) to model the *Fermi* LAT and radio LCs, and fit the predicted radio and γ-ray profiles to the data concurrently, thereby significantly constraining α and ζ. This also allows us to test the consistency of the various approaches used to infer the pulsar geometry.

2. Model

We use an idealized picture of the pulsar system, wherein the magnetic field has a retarded dipole structure [4] and the γ-ray emission originates in regions of the magnetosphere (referred to as 'gaps') where the local charge density is sufficiently lower than the Goldreich-Julian charge density [7]. These gaps facilitate particle acceleration and radiation. We assume that there are constant-emissivity emission layers embedded within the gaps in the pulsar's corotating frame. The location and geometry of these emission layers determine the shape of the γ-ray LCs, and there exist multiple models for the geometry of the magnetosphere describing different possible gap configurations.

We included two models for the γ-ray emission regions in this study, namely the Outer Gap (OG) and Two-Pole Caustic (TPC) models. In both the OG and TPC models (the Slot Gap model [1] may serve as physical basis for the latter), emission is produced by accelerated charged particles moving within narrow gaps along the last open magnetic field lines. In the OG model [3], radiation originates above the null charge surface (where the Goldreich-Julian charge density changes sign) and interior to the last open magnetic field lines. The TPC gap starts at the stellar surface and extends along the last open field lines up to near the light cylinder, where the corotation speed approaches the speed of light [5]. The special relativistic effects of aberration and time-of-flight delays, which become important in regions far from the stellar surface (especially near the light cylinder), together with the curvature of the magnetic field lines, cause the radiation to form caustics (accumulated emission in narrow phase bands). These caustics are detected as peaks in the observed γ-ray LC [5, 9].

We used an empirical radio cone model [11], where the beam diameter, width, and altitude are functions of the pulsar period P, its time derivative $\dot{P}$, and the frequency of observation ν, in order to obtain predictions for the radio LCs. This is different from the approach taken by [14], as we have a different prescription for the radio emission altitude and cone half opening angle, and we do not use the polarization data.

3. Method

Using the above geometric models, we generated LCs as a function of α and ζ, keeping the gap widths and extents constant. Due to the large size of the (α,ζ)-space at a $1°$ resolution, it is impractical to search blindly for the optimum LC by eye. We therefore started by generating a so-called atlas of LCs with a $10°$ resolution for each pulsar and first identified candidate LC fits. We then performed refined searches in the regions of (α,ζ)-space around those candidate fits at a $5°$ and later $1°$ resolution. This approach of generating all the LCs in a candidate region and comparing them directly, allowed us to obtain constraints on α and ζ. We then inferred contours for α and ζ for each pulsar and for each geometric model. We lastly used these contours to find the corresponding values of f_Ω (with errors; see Section 3.2) predicted by the OG and TPC models.

3.1. Obtaining the contours

To obtain an (α,ζ)-contour delimiting the region of plausible LC fits, we start at the candidate solution ($5°$ resolution) and first move away from it in steps of $1°$ in α. At each step we then step through ζ until the upper and lower bounds of the contour are located for the fixed α. This procedure is repeated until no further acceptable LCs are found. As an example, the coloured regions **A** and **B** in the left panel of Figure 1 indicate the resulting contours obtained in this manner for PSR J1509−5850 in the TPC case.

Oftentimes we find two disjoint solution contours, with one of the two sometimes producing a better LC fit. The example shown here is one of these cases, as can be seen from the representative LCs shown in Figure 1. Contour **B** yields a considerably better fit than contour **A**, and thus we can ignore contour **A** in favour of contour **B** as indicated by the dotted line in
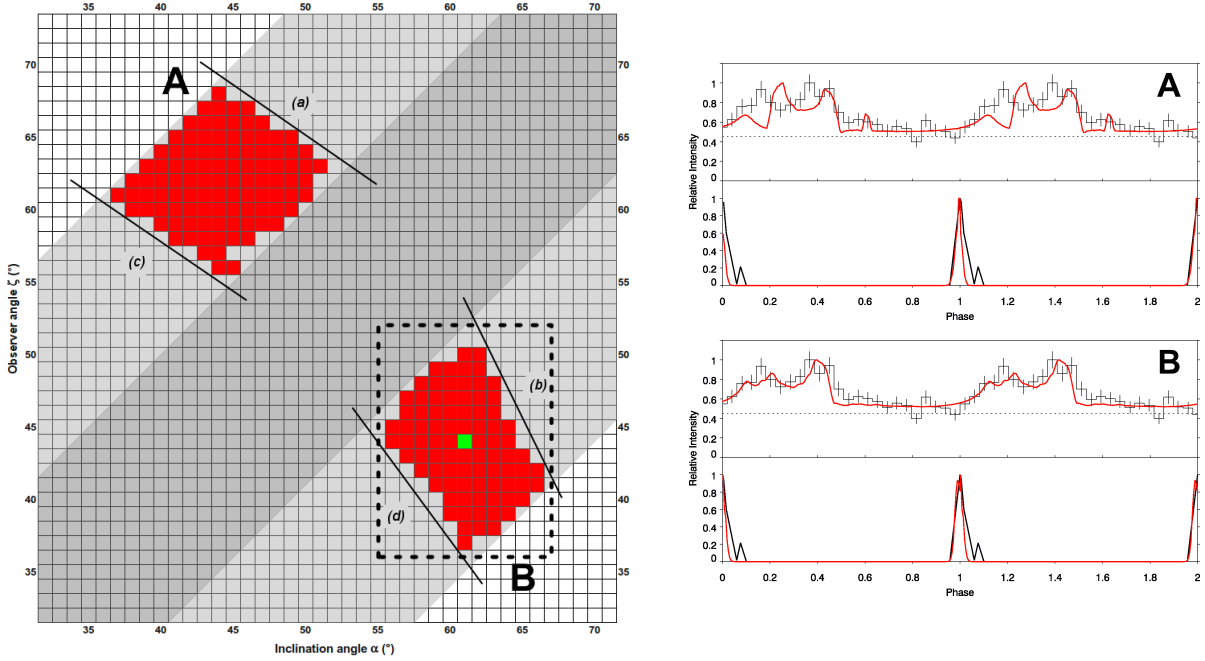
Figure 1. *Left:* The (α,ζ)-contours (regions **A** and **B**) for radio and γ-ray LC fits of PSR J1509−5850 for the TPC model (*red*). The dark grey and light grey regions correspond to double-peaked and single-peaked radio LCs respectively. The solid lines indicate approximately the locations of the boundaries to the contours due to: (*a*) the relative phase lag between the radio and γ-ray peaks being too large, (*b*) the bridge emission's relative intensity being too low, and (*c,d*) the γ-ray peak being too narrow. The dashed line (bounded area) indicates the resulting errors on α and ζ, with the *green* block indicating our best fit. *Right:* Representative LC fits corresponding to the contours **A** and **B**.

Figure 1. The values of α and ζ reported in Table 1 are those at the centre of this dotted box, while the errors on these values are conservatively chosen to be the dimensions of the box. In this case the resulting values are $\alpha = (61° \pm 5°)$ and $\zeta = (44° \pm 7°)$.

3.2. Finding f_Ω

It is important to be able to convert the observed energy flux of a pulsar to its all-sky luminosity. The flux correction factor f_Ω is used for this purpose. It is a highly model-dependent parameter, and allows us to determine what fraction of the all-sky luminosity we are observing from a pulsar if the geometry is known (α and ζ), for a given model. It is also crucial in deriving the γ-ray efficiency of a pulsar, and is defined as [13]

$$f_\Omega(\alpha, \zeta_E) = \frac{\iint F_\gamma\left(\alpha, \zeta, \phi\right) \sin \zeta d\zeta d\phi}{2 \int F_\gamma\left(\alpha, \zeta_E, \phi\right) d\phi},$$
(1)

with F_γ being the photon flux per solid angle ('intensity'), and ζ_E the Earth line-of-sight. (Note, we assume that $F_\gamma(\zeta, \phi)/F_{\gamma,\text{tot}}$ is approximately equal to the ratio of observed energy flux vs. total energy flux.)

We can now use the (α,ζ)-contours obtained by the method discussed in Section 3.1 to constrain the value of f_Ω by computing $f_\Omega(\alpha, \zeta)$ and overplotting those contours (see Figure 2).
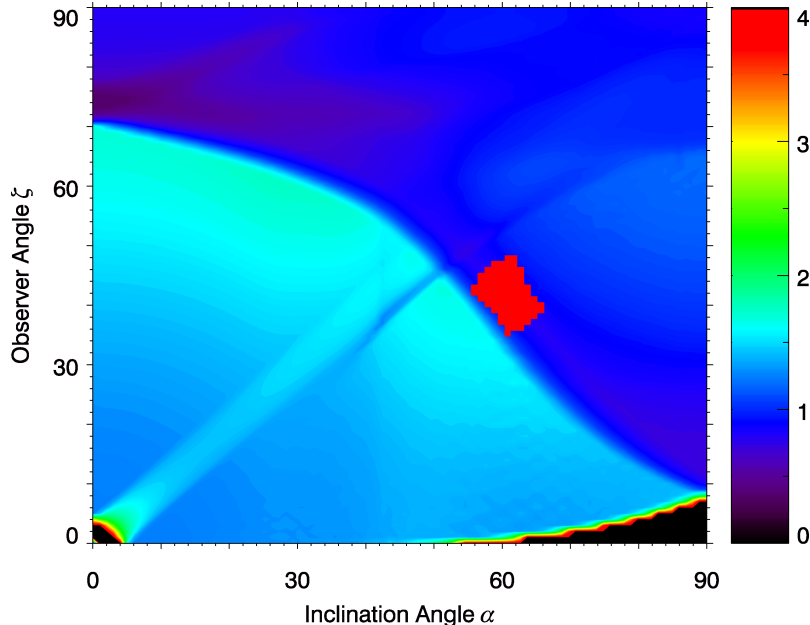
Figure 2. Contour plot of f_Ω as function of α and ζ implied by the TPC model for PSR J1509-5850. The *red* area indicates the best-fit (α, ζ)-contour for the radio and γ-ray LCs.

4. Results

We infer values for α and ζ for each pulsar with typical errors of $\sim 5°$ (see Table 1). The tabulated values are the average values of α, ζ, and β implied by the solution contours, while the errors are chosen conservatively so as to include the full (non-rectangular) contour. We note that once a solution is found at a particular α and ζ, it is worthwhile to study the LC at the position $\alpha' = \zeta$ and $\zeta' = \alpha$ (i.e., when the angles are interchanged). Such a complementary solution may provide a good fit in some cases (see the alternative solutions listed in Table 1), due to the symmetry of the model as well the symmetry in pulsar geometry (i.e., $|\beta|$ remaining constant under this transformation).

5. Discussion and Conclusions

The good constraints on α and ζ, obtained using the method described above, emphasizes the merit of a multiwavelength approach. For example, the light grey regions in Figure 1 indicate single-peaked radio profile LC solutions. These would represent typical constraints one would be able to derive for α and ζ when considering only the radio profile shapes. Similarly, when only considering the (single-peaked) γ-ray LCs, one would find relatively large (α,ζ)-contours [13]. The requirement of fitting both the radio and γ-ray profile shape, as well as their relative phase lag, result in much smaller contours, as shown in Figure 1.

The next step for this kind of study is to apply a mathematically rigorous method of determining the best-fit LC solutions as a function of many free model parameters to the six pulsars modelled in this paper. An example is the Markov chain Monte Carlo method which has been successfully applied to millisecond pulsar LCs [8].

References

[1] Arons J 1983 *ApJ* **266** 215–41
[2] Blaskiewicz et al. 1991 *ApJ* **370** 643–69
[3] Cheng K S, Ho C and Ruderman M 1986 *ApJ* **300** 500–21
[4] Deutsch A J 1955 *Ann. d'Astrophys.* **18** 1–10
[5] Dyks J and Rudak B 2003 *ApJ* **598** 1201–6
[6] Gil J, Gronkowski P and Rudnicki W 1984 *A&A* **132** 312–16
[7] Goldreich P and Julian W H 1969 *ApJ* **157** 869–80
[8] Johnson T J, Harding A K and Venter C 2011, in preparation
[9] Morini M 1983 *MNRAS* **202** 495–510
[10] Radhakrishnan V and Cooke D J 1969 *ApJL* **3** 225–29
[11] Story S A, Gonthier P L and Harding A K 2007 *ApJ* **671** 713–26
[12] Venter C, Harding A K and Guillemot L 2009 *ApJ* **707** 800–22
[13] Watters K P, Romani R W, Weltevrede P and Johnston S 2009 *ApJ* **695** 1289–1301
[14] Weltevrede P et al. 2010 *ApJ* **708** 1426–41

Table 1. Values for α, ζ, β, and f_Ω derived for the 6 pulsars for both the OG and TPC models.

Pulsar	Model	α (°)	ζ (°)	β (°)	f_Ω
J0631+1036	OG	74 ± 5	67 ± 4	$-\ 6 \pm 2$	0.93 ± 0.06
	TPC	71 ± 6	66 ± 7	$-\ 5 \pm 3$	1.04 ± 0.04
J0659+1414	OG	59 ± 3	48 ± 3	-12 ± 5	1.16 ± 0.53
	TPC	50 ± 4	39 ± 4	-13 ± 6	1.64 ± 0.04
	TPC[1]	38 ± 1	50 ± 4	11 ± 4	1.63 ± 0.05
J0742−2822	OG	86 ± 3	71 ± 5	-16 ± 6	0.99 ± 0.10
	OG[1]	71 ± 6	86 ± 4	16 ± 6	0.81 ± 0.09
	TPC	64 ± 8	80 ± 4	15 ± 6	0.88 ± 0.41
J1420−6048	OG	67 ± 5	45 ± 7	-22 ± 9	0.77 ± 0.13
	TPC	64 ± 6	43 ± 8	-21 ± 9	0.90 ± 0.10
	TPC[1]	42 ± 5	63 ± 5	21 ± 9	0.77 ± 0.06
J1509−5850	OG	66 ± 4	50 ± 7	-18 ± 8	0.77 ± 0.11
	TPC	61 ± 5	44 ± 7	-18 ± 8	0.89 ± 0.10
J1718+3825	OG	67 ± 6	48 ± 6	-19 ± 8	0.76 ± 0.12
	TPC	61 ± 5	43 ± 6	-19 ± 8	0.86 ± 0.07
	TPC[1]	42 ± 6	62 ± 5	19 ± 7	0.83 ± 0.10